Positron–hydrogen-atom S-wave coupled-channel scattering at low energies

B. J. Archer* and G. A. Parker
Department of Physics and Astronomy, University of Oklahoma, Norman, Oklahoma 73019

R. T Pack
Theoretical Division (T-12 MS J569), Los Alamos National Laboratory, Los Alamos, New Mexico 87545
(Received 31 March 1989)

Results are presented for both inelastic and rearrangement scattering of positrons by hydrogen atoms for total angular momentum of zero. Sector adiabatic basis functions in hyperspherical coordinates are used to form a 43-coupled-channel scattering expansion for energies below the H($n=4$) threshold. Partial cross sections out of $e^+ + H(1)$ into H(1), Ps(1), H(2), Ps(2), and H(3) are shown, as are those out of $p^+ + Ps(1)$ into H(2), Ps(2), and H(3). Considerable resonance structure is apparent in all of these cross sections.

I. INTRODUCTION

A positron scattering with a hydrogen atom is conceptually one of the simplest rearrangement processes; it results in positronium formation in addition to the usual elastic and inelastic processes. Positronium (Ps) is a hydrogenic atom consisting of an electron and a positron. If zero energy is defined by the ionization energy, the hydrogen state with a principle quantum number n has an energy of $-\mu_H/2n^2$ a.u., whereas the Ps energy levels are given by $-1/4n^2$ a.u. The reduced mass of hydrogen is $\mu_H=0.999\,456$ a.u. If the initial state is a positron plus a ground-state hydrogen atom, then four distinct energy regions exist. Between -0.5 and -0.25 a.u. only elastic scattering is possible. Between -0.25 and -0.125 a.u., the Ore gap, positronium formation is the only nonelastic process. Above -0.125 a.u. excited states of the final atom, either H or Ps, are energetically allowed. Above 0.0 a.u. ionization, or three-body breakup, is possible. This work will stay at scattering energies below three-body breakup. We use notation such as H(3) to denote the hydrogen atom $n=3$ states, and specify a particular angular momentum state by H($3p$).

There has been considerable theoretical interest in $e^+ + H$ for many years even though there are not yet any experimental results. For low energies Humberston has reviewed both the early works[1] and the current status of the problem.[2] Even after three decades of work this system is still relatively intractable with only the zero total angular momentum elastic phase shifts for energies below Ps formation known precisely.[3–16]

Results in the Ore gap, where both elastic scattering and Ps formation can occur, are not as consistent as for purely elastic scattering. Many calculations of the positronium-formation cross section[8–10,14,17–22] have been made but no two agree in both magnitude and shape. It is generally accepted that the results of Humberston[20] are the best to date, even after taking into account the 10% uncertainty he reports.[20(b)]

At energies greater than the opening of the H(2) channel, but below the ionization threshold, results are very sparse. In this energy range there have been calculations using the Born approximation[22] and the impulse approximation,[23,24] but both approximations are often inaccurate by as much as two orders of magnitude at energies this low.[2] A two-state calculation of the Ps(1) formation cross section[25] in this energy range gave results of the same order of magnitude as the Born approximation. Two calculations[18,26] have used a three-state approximation and ignored Ps formation to calculate the H(1)→H(2) partial cross section at one energy in the energy range of interest. None of these methods is expected to be accurate in this energy range.

Mittleman[27] has predicted a series of resonances below the threshold of each excited state for $e^+ + H$. The existence of the resonances has been confirmed numerically[14,28–33] and formally by Treml.[34] Resonance positions have been found below the thresholds of H(2),[14] Ps(2), and H(3),[32] and below H(4) and Ps(3).[33]

Only the total angular momentum of zero partial wave for positron–hydrogen-atom scattering is examined in this work. Scattering energies are varied between the elastic threshold and the threshold of H(4). Cross sections out of the initial state $e^+ + H(1)$ into Ps(1), H(2), Ps(2), and H(3) are reported, as are cross ections out of $p^+ + Ps(1)$ into H(2), Ps(2), and H(3). The reactive scattering method of Pack and Parker,[35,36] which uses adiabatically adjusting principal axis hyperspherical (APH) coordinates, has been modified and used for this Coulomb problem. Forty-three adiabatic basis functions, not asymptotic states, are used to solve the coupled-channel equations. An infinitely massive proton is *not* assumed, but spin effects are ignored.[37]

Section II provides a summary of the theory and calculations. Scattering results are presented in Sec. III, and Sec. IV concludes this work.

II. THEORY AND CALCULATIONS

The reactive scattering method of Pack and Parker has been published elsewhere;[35,36] thus, this section will con-

centrate on the application of the theory to three particles interacting via Coulomb potentials. APH coordinates[35,36] use three Euler angles to describe the tumbling motions of the plane defined by the three particles. Motion of the particles in the plane is described by three internal coordinates.

Supppose that two of the particles form an atom whose radial vector is $\mathbf{r}_i$ and that the vector from the center of mass of the atom to the third particle is $\mathbf{R}_i$. A set of mass scaled Jacobi coordinates[35,36] for the ith arrangment channel is then defined by

$$\begin{aligned} \mathbf{s}_i &= d_i^{-1}\mathbf{r}_i \ , \\ \mathbf{S}_i &= d_i\mathbf{R}_i \ , \\ \cos\Theta_i &= \mathbf{S}_i\cdot\mathbf{s}_i/S_i s_i \ , \end{aligned} \tag{1}$$

where the mass scaling factor is

$$d_i = \left[\frac{m_i}{\mu}\left[1-\frac{m_i}{M}\right] \right]^{1/2} . \tag{2}$$

The total mass is M, m_i is the mass of the separated particle, and the system reduced mass is given by

$$\mu = (m_A m_B m_C/M)^{1/2} . \tag{3}$$

APH coordinates,[35,36] which treat all three arrangement channels equally, are defined by

$$\begin{aligned} \rho &= (S_i^2+s_i^2)^{1/2} \ , \\ \tan\theta &= \frac{[(S_i^2-s_i^2)^2+(2\mathbf{S}_i\cdot\mathbf{s}_i)^2]^{1/2}}{2S_i s_i\sin^2\Theta_i} \ , \\ \tan 2\chi_i &= \frac{2\mathbf{S}_i\cdot\mathbf{s}_i}{S^2-s^2} \ . \end{aligned} \tag{4}$$

The hyperradius, which has units of length, gives a measure of how far apart the particles are and serves as the scattering coordinate, while the angular coordinates give the configuration of the particles. Ranges of the two hyperangles are $0\le\theta\le\pi/2$ and $0\le\chi_i<2\pi$. χ_i depends on i only by definition of the origin.

The kinetic energy operator is

$$T = T_\rho + T_h + T_r + T_C \ , \tag{5}$$

where the radial T_ρ, Coriolis T_C, and "hypersphere" T_h, terms are

$$\begin{aligned} T_\rho &= -\frac{\hbar^2}{2\mu\rho^5}\frac{\partial}{\partial\rho}\rho^5\frac{\partial}{\partial\rho} \ , \\ T_C &= -\frac{i\hbar\cos\theta}{\mu\rho^2\sin^2\theta}J_y\frac{\partial}{\partial\chi} \ , \\ T_h &= -\frac{\hbar^2}{2\mu\rho^2}\left[\frac{4}{\sin(2\theta)}\frac{\partial}{\partial\theta}\sin(2\theta)\frac{\partial}{\partial\theta}+\frac{1}{\sin^2\theta}\frac{\partial}{\partial\chi^2}\right] . \end{aligned} \tag{6}$$

The rotational term is written as

$$T_r = AJ_x^2 + BJ_y^2 + CJ_z^2 \ , \tag{7}$$

where the coefficients are

$$\begin{aligned} A(\rho,\theta) &= [\mu\rho^2(1+\sin\theta)]^{-1} \ , \\ B(\rho,\theta) &= (2\mu\rho^2\sin^2\theta)^{-1} \ , \\ C(\rho,\theta) &= [\mu\rho^2(1-\sin\theta)]^{-1} \ . \end{aligned} \tag{8}$$

Total angular momentum wave functions of good parity p are expanded in the form

$$\Psi^{JMpn} = 4\sum_{i,\Lambda}\rho^{-5/2}\psi_{i\Lambda}^{Jpn}(\rho)\Phi_{i\Lambda}^{Jp}(\theta,\chi;\rho_\xi)\hat{D}^{Jp}_{\Lambda M}(\alpha,\beta,\gamma) \ , \tag{9}$$

where $\hat{D}^{Jp}_{\Lambda M}$ is a normalized, good parity, Wigner rotation function[36] of the Euler rotation angles. The surface functions $\Phi_{i\Lambda}^{Jp}(\theta,\chi;\rho_\xi)$ are solutions of

$$\left[T_h + \frac{(A+B)}{2}\hbar^2 J(J+1) + \left[C - \frac{A+B}{2} \right]\hbar^2\Lambda^2 + \frac{15\hbar^2}{8\mu\rho_\xi^2} + V(\rho_\xi,\theta,\chi) \right] \Phi_{i\Lambda}^{Jp}(\theta,\chi;\rho_\xi) = \mathcal{E}_{i\Lambda}^{Jp}(\rho_\xi)\Phi_{i\Lambda}^{Jp}(\theta,\chi;\rho_\xi) \tag{10}$$

at fixed values of the hyperradius ρ_ξ. The three-body potential is just the sum of three Coulomb potentials

$$V(r_A,r_B,r_C) = -\frac{1}{r_A}-\frac{1}{r_B}+\frac{1}{r_C} \ , \tag{11}$$

where r_A is the distance between the proton and electron, r_B is the distance between the positron and electron, and r_C is the distance between the proton and positron. Inversion of Eq. (4) provides the radial distances r_i.[35–37] As has been described previously,[38,39] Eq. (10) was solved numerically using the finite-element method. For this work, solutions of Eq. (10) were found at 267 ρ_ξ in the range $0.3\le\rho\le 120.0$ a.u.

At small and medium hyperradii the surface functions have amplitude in most of the (θ,χ) plane and are not difficult to calculate with the finite-element method. However, at large hyperradii they take on the character of hydrogenic atomic states in the field of a distant charged particle. As the hyperradius increases two processes combine to reduce the area of significant amplitude. First, the surface functions take on the character of polarized atomic states localized in arrangement channels, with the lowest surface functions doing so before the higher functions. Second, in hyperspherical coordinates the area in the plane covered by each arrangement channel decreases as the hyperradius increases.

Combining these two effects we see from Fig. 1 that the lowest surface function takes on the character of the H(1s) state at moderate hyperradii and then localizes even more as the hyperradius increases. Similarly, the second surface functions takes on the character of the Ps(1s) state. However, the higher surface functions take on their atomic state character very slowly and have amplitude in large areas of the (θ,χ) plane until large hyperradii. By $\rho=120.0$ bohr the surface functions corresponding to H(3) states still cover about 10% of the plane. At the same hyperradius the lowest surface function has amplitude in less than 0.5% of the plane. Therefore, the method for calculating the surface functions

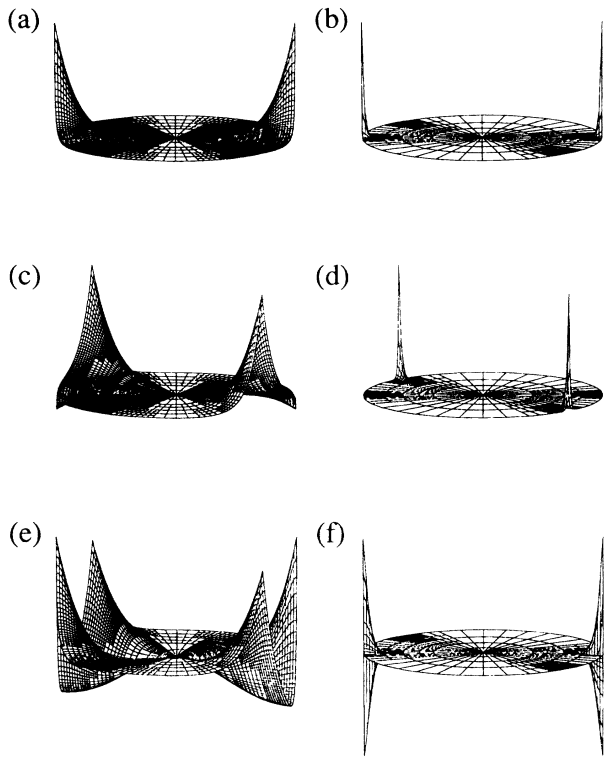

FIG. 1. Lowest three surface functions on grids that lack the finest spaced nodes of a production grid at $\rho=11.0$ bohr on the left and $\rho=120.0$ bohr on the right. Each arrangement channel is shown twice due to the symmetry behavior of χ. θ is zero at the center and is $\pi/2$ at the outer edge. χ is zero at the right-hand-side H arrangement channel, and is positive counterclockwise. The first and second surface functions show their localized H($n=1$) and Ps(1) characters in (b) and (d), respectively. Surface function 3 has amplitude in both the H and Ps arrangement channels in (e), and is a linear combination of the H($2s$) and H($2p$) states in (f).

must be able to simultaneously calculate both highly localized states and very delocalized states.

The finite-element method expands $\Phi_{t\Lambda}^{J^p}$ in second-order polynomials which are only defined on small regions of the (θ,χ) space called elements. Each element is a quadrilateral defined by nine grid points at which the polynomials are evaluated. Elements vary in size from large in areas of small amplitude to very small in areas of large amplitude. Taken together the elements form a highly nonuniform two-dimensional (2D) grid containing approximately 4000 nodes on the region $0\le\chi\le\pi$ rad, and $0\le\theta\le\pi/2$, with most of the nodes concentrated in areas of large amplitude in the surface functions.

At large hyperradii the lowest surface functions have a cusp at the nuclear singularity, see Fig. 1, which changes so rapidly it is difficult to fit with polynomials, while at the same hyperradius the higher functions have exponential tails which cover a large fraction of the space. To improve the accuracy of the lowest surface functions a new set of surface functions was defined by removing exponential factors from the original surface functions,

$$\bar{\Phi}=\Phi\sum_{i=1}^{2}\exp(\beta_i s_i)\ , \tag{12}$$

where i is the arrangement channel (H or Ps). In Eq. (12) the scaling factors were chosen as $\beta_1=0.85$ and $\beta_2=0.55$, intermediate values between those required to match the $n=1$ and $n=2$ exponential factors of the respective atoms. Partially removing the exponential behavior of the lowest atomic states made it possible to calculate the energies of the lowest surface functions with about 1% accuracy.

Partial removal of the exponential tails by Eq. (12) increases the amplitude of the higher $\bar{\Phi}$ far from the singularities causing them to be quite dependent on the accuracy of the tails. The total number of nodes in the gird was limited by about 4000 due to memory limitations, and most of the nodes were used to construct a fine grid near the singularities in the potential. Therefore, it was difficult to get enough nodes into the tails of the $\bar{\Phi}$ for $t\ge 10$, which limits the maximum scattering energy to just above the H(3) threshold.

For this work a good expansion of the scattering wave functions was provided by calculating the energies of the lowest nine surface functions with the aforementioned 1% accuracy and carrying an additional 34 surface functions for convergence. Asymptotically the lowest nine surface functions correspond to the hydrogen atomic states through $n=3$ and positronium atomic states through $n=2$. The surface functions were computed at many hyperradii and were used as a sector adiabatic basis for the coupled-channel calculation. By sector adiabatic basis we mean that each set of $\Phi(\rho_\xi)$ was used as the scattering basis for a small range of hyperradii, called a sector, centered on ρ_ξ.

Orthonormality of the basis functions results in coupled-channel scattering equations

$$\left[\frac{\partial^2}{\partial\rho^2}+\frac{2\mu}{\hbar^2}E\right]\psi_{t\Lambda}^{J^pn}(\rho)$$
$$=\frac{2\mu}{\hbar^2}\sum_{t',\Lambda'}\langle\Phi_{t\Lambda}^{J^p}\hat{D}^{J^p}_{\Lambda M}|H_i|\Phi_{t'\Lambda'}^{J^p}\hat{D}^{J^p}_{\Lambda' M}\rangle\psi_{t'\Lambda'}^{J^pn}(\rho)\ , \tag{13}$$

where E is the total energy, $V(\rho,\theta,\chi)$ is the three-body potential, and

$$H_i=T_h+T_r+T_c+\frac{15\hbar^2}{8\mu\rho^2}+V(\rho,\theta,\chi)\ . \tag{14}$$

All the coupling has been retained in the scattering equations resulting in a set of 43 coupled-channel equations. Equation (13) was propagated over the range $0.3\le\rho\le 120.0$ bohr using the logarithmic derivative method.[40]

In the method of Pack and Parker,[35,36] once propagation is finished the APH R matrix is transformed to Delves[41] coordinates and the boundary conditions are applied. The only changes required in the scattering step for Coulomb-type problems occur in the APH-to-Delves transformation and in applying the boundary conditions.

The APH-to-Delves transformation and the application of the boundary conditions require Delves atomic wave functions and integrals over Delves coordinates. Delves wave functions are calculated numerically because

the atoms are polarized by the field of the third particle. Expansion of the Delves functions in hydrogenic states is not appropriate because only 81.4% (Ref. 42) of the hydrogen atom polarization can be accounted for by hydrogen-atom bound states. Instead, Sturmian functions[43,44] which form a discrete, orthonormal, and complete basis are used. Sturmians are given by

$$\Lambda_{kl}(x)=\left[\frac{\gamma_i k!}{(n+l+1)!}\right]^{1/2} x^{l+1}e^{-x/2}L_k^{2l+2}(x)\ , \qquad (15)$$

where $k=n-l-1$ and the argument is $x=\gamma_i s_i$. The mass scaled coordinate is related to Delves coordinates[35,36] by $s_i=\rho\sin\Theta_D$ and the mass-dependent factor is

$$\gamma_i=\frac{2\mu\eta}{d_i}\ . \qquad (16)$$

We chose the scaling facotr $\eta=1.0$ to assure a good expansion of the H($1s$) and Ps($1s$) states, although it can be assigned any real value.

We evaluated Delves coordinate integrals numerically using a Gauss-Laguerre quadrature,[45] with the same weights and zeros in both arrangement channels. The weights and zeros of the quadrature were chosen as a compromise between those required by each channel.

Surface functions and matrix elements are energy independent; thus scattering calculations can be performed at many energies once the basis functions Φ are found at all hyperradii. Calculations were performed at about 500 scattering energies with a spacing of about 5.0×10^{-3} a.u. away from thresholds, about 3.5×10^{-4} a.u. near the Ps(1), Ps(2), and H(3) thresholds, and about 1.5×10^{-4} a.u. near the H(2) threshold.

III. RESULTS

A plot of the surface function eigenvalues $\mathcal{E}_{l0}^{00}(\rho_\xi)$ versus hyperradius is given in Fig. 2 for $\rho\leq40.0$ a.u. The lowest few curves correspond to those of Refs. 14, 32, and 46. These adiabatic curves approach the energy levels of isolated H and Ps atoms asymptotically.

As can be seen from Fig. 3, the present elastic phase shifts differ from the previous results at the lowest energies, but agree reasonably well as higher energies. Convergence at the elastic threshold would be improved by decreasing the sector sizes or by using more surface functions in the scattering basis. Our main interest is in rearrangement and inelastic processes, and the elastic phase shifts are already well known,[3–16] so the additional expense did not seem justified. Further, as the scattering energy increases, convergence improves and our phase shifts rapidly approach the results of previous calculations.

The first energetically allowed nonelastic process is the rearrangement collision $e^+ + H(1)\rightleftharpoons p^+ + Ps(1)$. Between $k=0.7069$ and $0.8658a_0^{-1}$, the Ore gap, only elastic scattering and ground-state Ps formation are possible. Table I compares our elastic and Ps-formation eigenphase shifts and cross sections to those of Humberston.[20(a)] Eigenphase shifts corresponding to elastic scattering for energies in the Ore gap are shown in Fig. 3 and compared to those of Ref. 20(a).

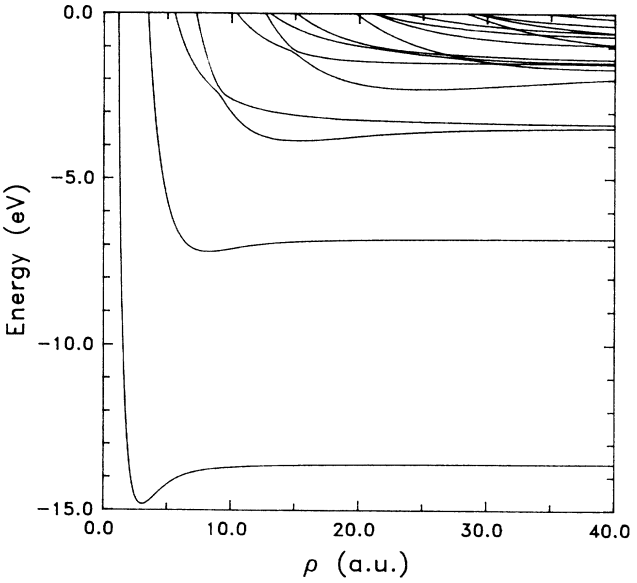

FIG. 2. Lowest 16 eigenvalues of the sector adiabatic basis vs ρ. The lowest four curves go to the H(1), Ps(1), and H(2) atomic energies asymptotically.

Figure 4 shows the $e^+ + H\rightarrow p^+ + Ps(1)$ partial cross section for $J=0$ in the Ore gap as calculated by several groups. Error analysis[37] indicates that our results are converged to within 2% with respect to the number of surface functions, but convergence with respect to the sector sizes is about 4%. Humberston,[20(a)] considered the

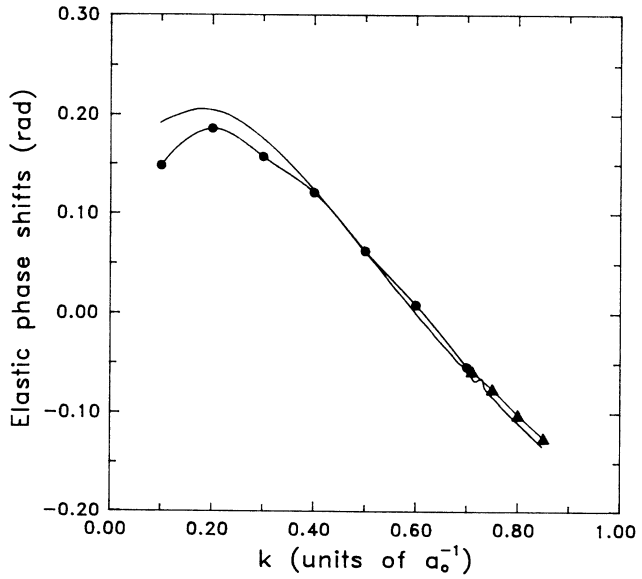

FIG. 3. Eigenphase shifts corresponding to elastic scattering through the Ore gap. Present results are the unmarked solid curve, Abdel-Raouf [Ref. 13(a)] is marked by ●, and Humberston [Ref. 20(a)] by △. The Ps(1) formation threshold is at $k=0.7069a_0^{-1}$, just before the slight structure in the present phase shifts.

TABLE I. Eigenphase shifts and cross sections out of $e^+ + H(1s)$ into elastic and ground-state positronium-formation channels in the Ore gap.

k (a_0^{-1})	δ_H (rad)	δ_{Ps} (rad)	σ_H (πa_0^2)	σ_{Ps} (πa_0^2)
0.71[a]	−0.065	0.362	0.033	0.0034
0.71[b]	−0.058	0.350	0.026	0.0041
0.75[a]	−0.084	−0.487	0.050	0.0038
0.75[b]	−0.076	−0.491	0.043	0.0044
0.80[a]	−0.110	−0.984	0.076	0.0043
0.80[b]	−0.102	−0.988	0.065	0.0049
0.85[a]	−0.135	−1.308	0.100	0.0049
0.85[b]	−0.125	−1.310	0.086	0.0058

[a]Present results.
[b]Reference 20(a).

most accurate to date with a possible 10% error,[20(b)] is 20% higher than the present results but has about the same qualitative shape. From Fig. 4 it is clear that all other calculations of Ps formation in the Ore gap differ from the present results and Humberston,[20] and each other, either qualitatively or quantitatively.

The Ps(1s) partial cross section is shown in Fig. 5 for energies from the formation threshold to just below the H(4) threshold using a fine energy grid. There is considerable structure in this cross section related to new channels opening and resonances associated with those channels. At the Ps(1) threshold the cross section rises very steeply, which is in agreement with Humberston.[20] For $\rho < 6.0$ a.u. the H and Ps energies are above the barrier between the H and Ps arrangement channels, therefore

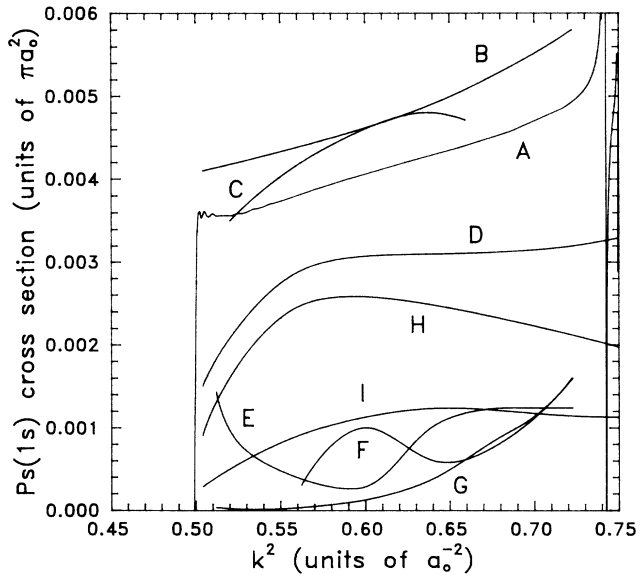

FIG. 4. Partial cross section for $J=0$ Ps($n=1$) formation for energies in the Ore gap. *A*, present results; *B*, Humberston [Ref. 20(a)]; *C*, Stein and Sternlicht (Ref. 8); *D*, Chan and Fraser (Ref. 10); *E*, Wakid (Ref. 9); *F*, Dirks and Hahn (Ref. 17) ($\times 10$); *G*, Wakid and LaBahn (Ref. 19) ($\times 10$); *H*, Khan and Ghosh (Ref. 21) ($\times 10^{-1}$); *I*, first Born from Khan and Ghosh (Ref. 21) ($\times 10^{-3}$). The Ps(1) threshold is at $k^2=0.4997a_0^{-2}$ and the H(2) threshold is at $k^2=0.7496a_0^{-2}$.

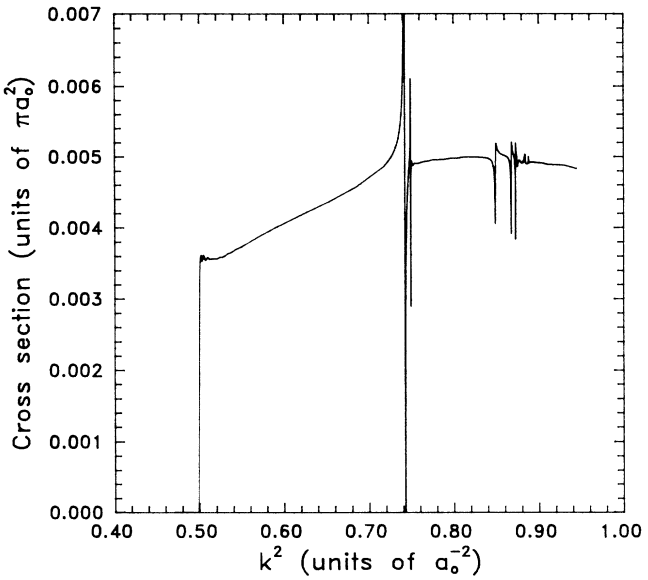

FIG. 5. Partial cross section for $e^+ + H(1) \rightarrow p^+ + Ps(1)$ from the Ps-formation threshold to just below the H(4) inelastic threshold. The clipped structure has a maximum magnitude of $0.0712\pi a_0^2$ and a minimum of $5.467\times 10^{-6}\pi a_0^2$.

Ps(1) forms as soon as it is energetically allowed. Slight oscillations due to incomplete convergence broaden the Ps(1) partial cross section at the formation threshold in Fig. 5.

Excitation of H into $n=2$ is possible starting at $k^2=0.7496a_0^{-2}$, and the first two structures from the left in Fig. 5 are associated with the opening of the H(2) channel. Figure 6 shows the Ps(1) partial cross section from the H(2) threshold to our highest scattering energy $k^2=0.93a_0^{-2}$. Also shown are the cross sections for excitation of hydrogen from the ground state to H(2s) and H(2p). From Fig. 6 we see that the second structure from the left is due to the H(2) channel opening and that the first structure is a resonance below the H(2) threshold. To identify the structures above $k^2=0.75a_0^{-2}$ the H(3) and Ps(2) states must be examined.

Figure 7 shows the partial cross sections out of $e^+ + H(1s)$ into Ps(2s), Ps(2p), H(3s), H(3p), and H(3d). Threshold of the Ps(2) channel is at $k^2=0.8745a_0^{-2}$ and the threshold of the H(3) channel is at $k^2=0.8884a_0^{-2}$. There is a resonance in the H(3) channel which causes the strong dip in the Ps(2) partial cross sections at about $k^2=0.884a_0^{-2}$. These three features account for the three small peaks in Fig. 6 between $k^2=0.8745a_0^{-2}$ and $k^2=0.8884a_0^{-2}$. Remaining in Fig. 6 between $k^2=0.84a_0^{-2}$ and $k^2=0.8745a_0^{-2}$ are three structures which result from sharp resonances in the Ps(2) channel.

The inelastic partial cross sections appear to be converged to within 4% with respect to the number and spacing of surface functions, except near thresholds where the error may be 8%.[37] The cross section into the Ps(1) state appears to be converged to better than 4% with respect to the final scattering distance,[37] but the excited states are not as well converged. Asymptotically

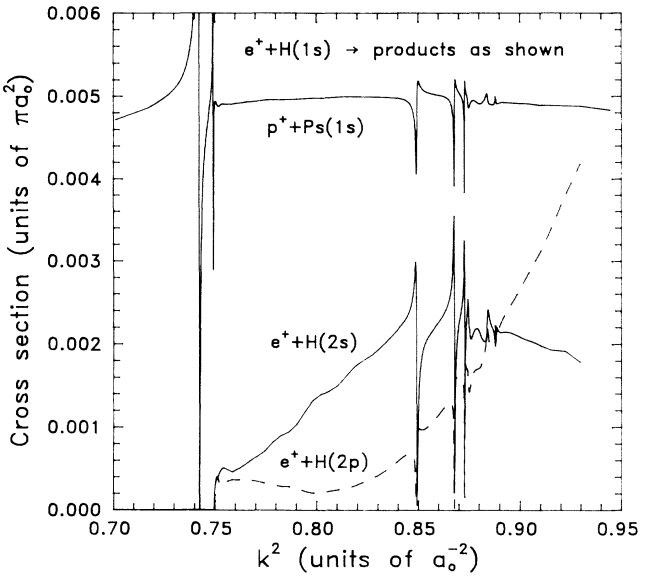

FIG. 6. $J=0$ partial cross sections out of H($1s$) from the H(2) threshold to the H(4) threshold. The upper solid curve is into Ps($1s$) and the lower curves are into H($2s$), lower solid curve, and H($2p$), dashed curve.

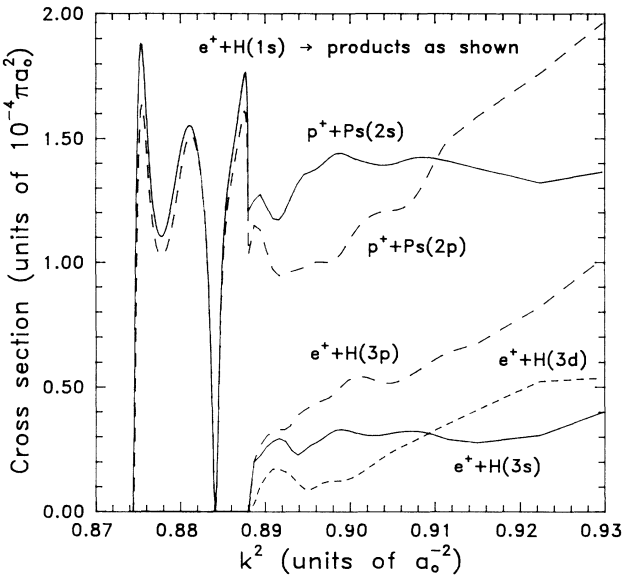

FIG. 7. $J=0$ partial cross sections out of H($1s$) from the Ps(2) threshold to the H(4) threshold. The upper two curves are into Ps($2s$), solid, and Ps($2p$), dashed, whereas the lower three curves are into H($3s$), lower solid; H($3p$), lower dashed; and H($3d$), short dashed.

the hydrogenic excited states are degenerate. However, at moderate distances the electric field from the charged particles causes these states to split. This prevents accurate application of the usual sine- and cosine-type boundary conditions[47–49] until large scattering distances have been reached. Scattering propagation was stopped at $\rho=120.0$ a.u. and the usual boundary conditions were applied. Convergence tests indicate that this causes an approximately 15% error[37] in the excited-state partial cross sections. For a thorough discussion of the error analysis see Ref. 37.

Table II shows the estimated positions of the five resonances identified from our scattering calculation and compares them to previous predictions of these positions.[14,32] Resonance positions are estimated from the scattering calculation by averaging the positions of the two points with the largest and smallest cross section in each resonance. The lowest resonance found below the Ps($n=2$) threshold is at $E=-0.074\,95$ a.u., which agrees with that of Ho and Greene.[32] Doolen[30] reported a resonance at $E=-0.111$ a.u. for which we found no evidence, although the avoided crossing of the H($n=2$) states at $E=-0.09$ a.u. causes a "resonance" if the calculation has insufficient accuracy. Our scattering energies are spaced finely enough near thresholds that any structure wider than 3.5×10^{-4} a.u. will be evident: thus any resonances missed by this calculation must be quite narrow.

Bound states of diabatic energy curves, formed by allowing curve crossings to occur in Fig. 2, correspond to metastable states in the scattering calculation. Metastable states were calculated by a method similar to that of Ref. 14 and were used to help identify the above resonances. Two additional metastable states were found at $-0.038\,92$ and $-0.033\,77$ a.u. They belong to the H(4), Ps(3) set of diabatic curves but cannot be positively identified due to the multiple curve crossings and long-range nature of those states. These two metastable states correspond to the two resonances of Ref. 33 at $-0.038\,53$ and $-0.033\,93$ a.u., identified therein as the lowest Ps(3) and H(4) resonances, respectively.

Partial cross sections out of the initial state $p^+ + \mathrm{Ps}(1s)$ for $J=0$ are shown in Figs. 8 and 9. Included are the H(2), H(3), and Ps(2) final states for energies below the H(4) threshold. Zero energy for these cross sections was taken as the Ps(1) threshold, not the H(1) threshold used previously. These cross sections may also be in error by approximately 15% due to the long-range potentials of the excited states.

IV. CONCLUSIONS

We have presented coupled-channel results for the $J=0$ partial wave for positron–hydrogen-atom scatter-

TABLE II. Resonance positions for the lowest five states of $e^+ + \mathrm{H}$ from the scattering calculation. Zero energy is at the ionization threshold.

State	Previous (a.u.)	Present (a.u.)
H($1s$)	none	none
Ps($1s$)	none	none
H($2s$)	$-0.128\,51$[a]	$-0.128\,53$
Ps($2s$)	$-0.075\,14$[b]	$-0.074\,95$
Ps($2s$)	$-0.065\,83$[b]	$-0.065\,63$
Ps($2s$)	$-0.063\,39$[b]	$-0.063\,03$
H(3)	$-0.058\,03$[b]	$-0.057\,46$
H(3)	$-0.056\,03$[b]	

[a]Reference 14.
[b]Reference 32.

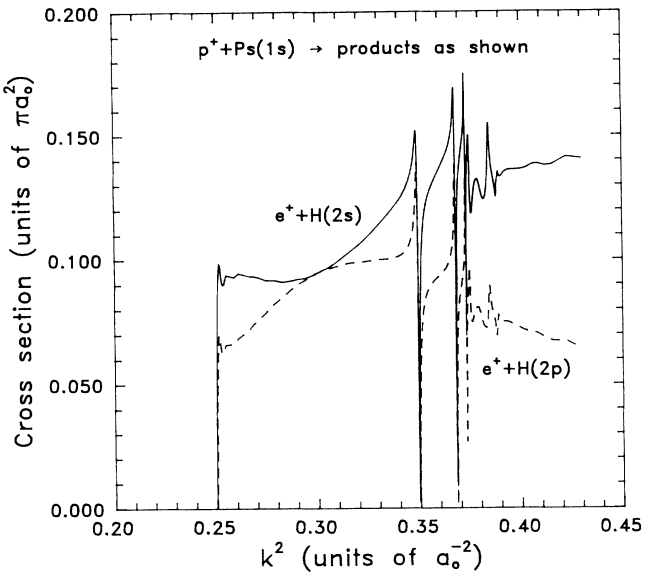

FIG. 8. $J=0$ Partial cross sections out of Ps($1s$) from the H(2) threshold to the H(4) threshold. The curves are into H($2s$), solid curve and H($2p$), dashed.

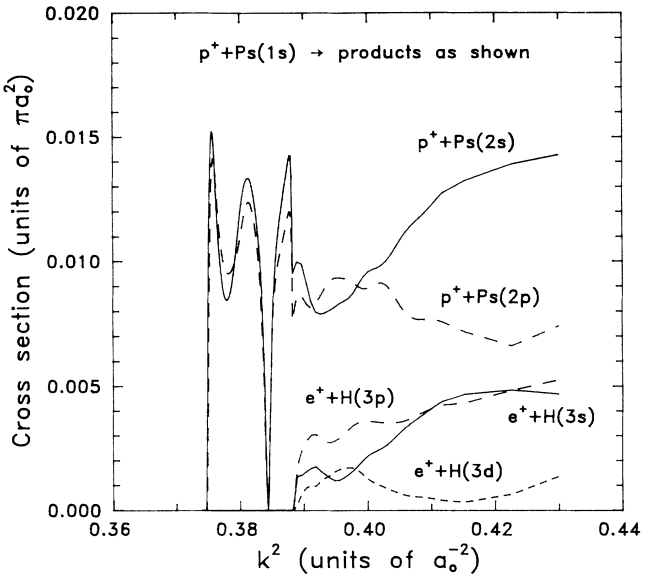

FIG. 9. $J=0$ partial cross sections out of Ps($1s$) from the Ps(2) threshold to the H(4) threshold. The upper two curves are into Ps($2s$), upper solid, and Ps($2p$), upper dashed, whereas the lower three curves are into H($3s$), lower solid; H($3p$), lower dashed; and H($3d$), short dashed.

ing at energies between the elastic threshold and the H(4) excited state. The $e^+ + \mathrm{H}(1) \rightarrow p^+ + \mathrm{Ps}(1)$ partial cross section is in reasonable agreement with that of Humberston[20] in the Ore gap and has been extended to excited-state scattering energies. Partial cross sections out of $e^+ + \mathrm{H}(1)$ into the H(2) and H(3) excited states are shown, as is the Ps(2) formation cross section. Elastic scattering is the dominant process followed by Ps(1) formation. The H(2) partial cross section is approximately an order of magnitude smaller than the Ps(1) partial cross section. Similarly, each partial cross section, inelastic or rearrangement, is approximately an order of magnitude smaller than the previous energetically allowed one. Also shown are partial cross sections of $p^+ + \mathrm{Ps}(1)$ into the H(2), H(3), and Ps(2) final states.

Five resonances due to metastable states are evident in the above partial cross sections. These resonances are within 1% of the previously predicted resonance positions.[14,32]

The discrete variable representation[50] and/or an expansion in analytic basis functions are currently being examined as replacements for the finite-element method in calculating the adiabatic basis functions. These methods speed up the calculation of the adiabatic basis functions as well as increasing their accuracy.[38] Extension of this work to higher partial waves is contemplated with the successful conclusion of that work and with the completion of a long-range propagator.

ACKNOWLEDGMENTS

We thank Dr. Robert Walker for the use of his 2D graphics programs, Melvin L. Pruiett for the use of his 3D graphics programs, and William A. Cook for assistance with the finite-element code. This work was partially supported by Associated Western Universities, National Science Foundation, Grant No. CHE-870-6385, and in part under the auspices of the U.S. Department of Energy.

*Present address: Center for Naval Analyses, 4401 Ford Avenue, P.O. Box 16268, Alexandria, VA 22302-0268.

[1]J. W. Humberston, Adv. At. Mol. Phys. **15**, 101 (1979).
[2]J. W. Humberston, in *Positron (Electron)-Gas Scattering*, edited by W. E. Kauppila, T. S. Stein, and J. M. Wadehra (World Scientific, Singapore, 1985), pp. 35–60.
[3]C. Schwartz, Phys. Rev. **124**, 1468 (1961).
[4]A. K. Bhatia, A. Temkin, R. J. Drachman, and H. Eiserike, Phys. Rev. A **3**, 1328 (1971).
[5]S. K. Houston and R. J. Drachman, Phys. Rev. A **3**, 1335 (1971).
[6]G. Doolen, G. McCartor, F. A. McDonald, and J. Nuttall, Phys. Rev. A **4**, 109 (1971).
[7]J. W. Humberston and J. B. G. Wallace, J. Phys. B **5**, 1138 (1972).
[8]J. Stein and R. Sternlicht, Phys. Rev. A **6**, 2165 (1972).
[9]S. E. A. Wakid, Phys. Rev. A **8**, 2456 (1973).
[10]Y. F. Chan and P. A. Fraser, J. Phys. B **6**, 2504 (1973).
[11]D. Register and R. T. Poe, Phys. Lett. **51A**, 431 (1975).
[12]J. R. Winick and W. P. Reinhardt, Phys. Rev. A **18**, 910 (1978).
[13](a) M. A. Abdel-Raouf, J. Phys. B **12**, 3349 (1979); (b) Can. J. Phys. **60**, 577 (1982).
[14]E. Pelikan and H. Klar, Z. Phys. A **310**, 153 (1983).

[15]H. Nakanishi and D. M. Schrader, Phys. Rev. A **34**, 1810 (1986).
[16]F. S. Levin and J. Shertzer, Phys. Rev. Lett. **61**, 1089 (1988).
[17]J. F. Dirks and Y. Han, Phys. Rev. A **3**, 310 (1971).
[18]G. J. Seiler, R. S. Oberoi, and J. Callaway, Phys. Rev. A **3**, 2006 (1971).
[19]S. E. A. Wakid and R. W. LaBahn, Phys. Rev. A **6**, 2039 (1972).
[20](a) J. W. Humberston, Can. J. Phys. **60**, 591 (1982); (b) J. Phys. B **17**, 2353 (1984).
[21]P. Khan and A. S. Ghosh, Phys. Rev. A **27**, 1904 (1983).
[22]H. S. W. Massey and C. B. O. Mohr, Proc. Phys. Soc. London **67**, 695 (1954).
[23]I. M. Cheshire, Proc. Phys. Soc. London **83**, 227 (1964).
[24]C. K. Majumdar and A. K. Rajagopal, Phys. Rev. **184**, 144 (1969).
[25]B. H. Bransden and Z. Jundi, Proc. Phys. Soc. London **92**, 880 (1967).
[26]P. G. Burke, H. M. Schey, and K. Smith, Phys. Rev. **129**, 1258 (1963).
[27]M. H. Mittleman, Phys. Rev. **152**, 76 (1966).
[28]S. E. A. Wakid, Phys. Lett. **54A**, 103 (1975).
[29]G. D. Doolen, J. Nuttall, and C. J. Wherry, Phys. Rev. Lett. **40**, 313 (1978).
[30]G. D. Doolen, Int. J. Quantum Chem. **14**, 523 (1978).
[31]L. T. Choo, M. C. Crocker, and J. Nuttall, J. Phys. B **11**, 1313 (1978).
[32]Y. K. Ho and C. H. Greene, Phys. Rev. A **35**, 3169 (1987).
[33]Y. K. Ho, in *Atomic Physics with Positrons,* edited by J. W. Humberston and E. A. G. Armour (Plenum, New York, 1987), pp. 411 and 412.
[34]T. F. Treml, Can. J. Phys. **63**, 941 (1985).
[35]R. T Pack, Chem. Phys. Lett. **108**, 333 (1984).
[36]R. T Pack and G. A. Parker, J. Chem. Phys. **87**, 3888 (1987).
[37]B. J. Archer, Ph.D. thesis, University of Oklahoma, 1988 (unpublished).
[38]G. A. Parker, R. T Pack, A. Laganà, B. J. Archer, J. D. Kress, and Z. Bačić, in *Proceedings of the NATO Advanced Workshop on Supercomputer Algorithms for Reactivity, Dynamics, and Kinetics of Small Molecules,* Vol. 277 of *NATO Advanced Study Institute, Series C: Mathematical and Physical Sciences,* edited by A. Laganà (Reidel, Dordrecht, 1989), p. 105.
[39]J. D. Kress, G. A. Parker, R. T Pack, B. J. Archer, and W. A. Cook, Comput. Phys. Commun. **53**, 91 (1989).
[40]B. R. Johnson, J. Chem. Phys. **67**, 4086 (1977); **69**, 4678 (1978).
[41]L. M. Delves, Nucl. Phys. **9**, 391 (1959); **20**, 275 (1960).
[42]M. Inokuti, Argonne Natonal Laboratory Report No. ANL-6769, 1964 (unpublished).
[43]H. Shull and P. O. Löwdin, J. Chem. Phys. **23**, 1362 (1955).
[44]P. O. Löwdin, Adv. Chem. Phys. **2**, 207 (1959), pp. 274–276.
[45]*Handbook of Mathematical Functions,* edited by M. Abramowitz and I. A. Stegun (Dover, New York, 1968).
[46]C. D. Lin and X. Liu, Phys. Rev. A **37**, 2749 (1988).
[47]M. J. Seaton, Proc. Phys. Soc. London **77**, 174 (1961).
[48]M. Gailitis and R. Damburg, Proc. Phys. Soc. London **82**, 192 (1963).
[49]M. Gailitis, J. Phys. B **9**, 843 (1976).
[50]J. V. Lill, G. A. Parker, and J. C. Light, Chem. Phys. Lett. **89**, 483 (1982); J. C. Light, I. P. Hamilton, and J. V. Lill, J. Chem. Phys. **82**, 1400 (1985).